Advances in real-time MR temperature mapping of the human heart

S. Roujol[1], B. denis de Senneville[1], G. Maclair[1], S. Hey[1], P. Jais[1], C. Moonen[1], and B. Quesson[1]
[1]CNRS/Université Bordeaux 2, Laboratory for Molecular and Functional Imaging, Bordeaux, France

Purpose/Introduction

The endocardiac treatment of heart arrhythmias by catheter radiofrequency ablation has become a clinically accepted therapy [1]. The efficiency and safety of the ablation is directly related to the delivered thermal dose, which is a function of temperature increase and exposure time. However, the absence of tissue temperature monitoring during RF delivery is a significant limitation. Magnetic Resonance Imaging (MRI) can provide rapid and quantitative thermometric measurements in addition to a detailed anatomical information. However, thermometry in the heart remains difficult because of the influence of 3D complex motion, including heart contraction and respiration. It has been proposed to simultaneously trigger the acquisition on both the cardiac cycle and respiration [2], at the cost of a loss in the temporal resolution of the thermometry. To overcome this limitation, we propose in the present study a method for monitoring the temperature evolution in the heart at each cardiac cycle. For this purpose, cardiac triggering and dynamic navigator-based slice tracking were combined with image registration and modeling of susceptibility changes with respiration, in order to investigate the precision of the thermometry on healthy volunteers.

Material and Methods

Healthy volunteers (N=19) were positioned head first in supine position in a 1.5 Tesla scanner (Philips Achieva/Intera) and a 5 element cardiac coil was used for image acquisition. The precision of the thermometry was evaluated in the left ventricle of the heart, using the short axis orientation for the temperature imaging slices. The sequence was triggered on the cardiac cycle with surface Electrocardiogramm (ECG) to acquire images in the mid or end diastole cardiac phase. The slice location was dynamically adjusted using a pencil-beam navigator positioned at the liver/lung interface (slice tracking technique) to compensate for respiratory motion. Combination of cardiac triggering and slice tracking allowed for the acquisition of 5 adjacent slices within a single cardiac cycle. Saturation slabs were positioned on each side of the imaging stack to reduce the intensity of blood signal. Each slice was acquired with a multishot Echo planar Imaging (EPI) sequence with the following parameters: 250x160 mm² rectangular Field of View (FOV), 96x96 matrix, 35 lines acquired per TR, 7 mm slice thickness, TE/TR=20/35 ms.

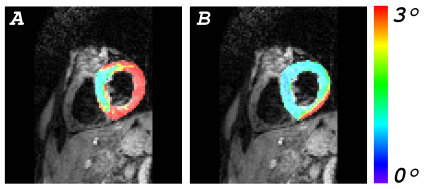

Figure 1 : Example of temperature standard deviation maps without (A) and with (B) correction (Volunteer 3)

For each volunteer, 200 acquisitions were repeated to cover several respiratory and cardiac cycles. Magnitude and phase images were processed offline to estimate the precision of the thermometry with the Proton Resonant Frequency (PRF) shift technique [3]. Despite compensation of cardiac and respiratory motions by cardiac triggering and slice tracking, potential jitter in the cardiac cycle period over the examination time could occur. Moreover, since slice tracking was performed only in the slice direction, in-plane image registration was required. In addition, local susceptibility changes related to lung volume modifications and liver displacement have to be compensated for in the phase images of the time series prior to temperature calculation with the PRF technique. To integrate all these constraints, the image processing was performed with the following steps:

Step 1. learning phase: In-plane motion compensation was performed by analyzing local displacements on the magnitude images. For this purpose, the first image in the time series was selected as the reference image, on which a region of interest (ROI) delimiting the left myocardium was manually drawn. A gradient driven descent algorithm maximizing the inter-correlation coefficient between this reference image and each following magnitude image of the time series was performed, assuming an affine displacement restricted to the selected ROI. The 6 coefficients of the affine transformation leading to the highest correlation with the reference image were stored for each image of the time series to create a list of reference values (C_i^t). From these coefficients, parametric phase maps were created, assuming a linear relationship between respiratory motion and susceptibility related phase changes. These synthetic phase images ($P_i(x,y)$) were computed by a Singular Value Decomposition (SVD) of the list of motion registered acquired phase ($\varphi_t(x,y)$) images with the coefficients using the following linear relationship:

$$\varphi_t(x,y) = \sum C_i^t P_i(x,y) + P_m(x,y), \qquad (1)$$

where $P_m(x,y)$ is an additional phase image representing the constant phase value of the fit. The registration of $\varphi_t(x,y)$ was performed on real and imaginary images using a bilinear interpolation (to avoid phase wraps).

Step 2. Thermometry: For each image acquired after the learning phase, the transformation coefficients calculated from registration of the magnitude image (gradient descent method with maximization of the intercorrelation coefficient) were applied on the $P_i(x,y)$ obtained as described in step 1 to compute a synthetic phase map with equation (1). This phase map was subtracted to the acquired motion registered phase image to suppress the background phase information prior to temperature calculation. The resulting motion registered and susceptibility compensated temperature maps were then processed to estimate the standard deviation in time for each pixel of the selected ROI covering the left myocardium.

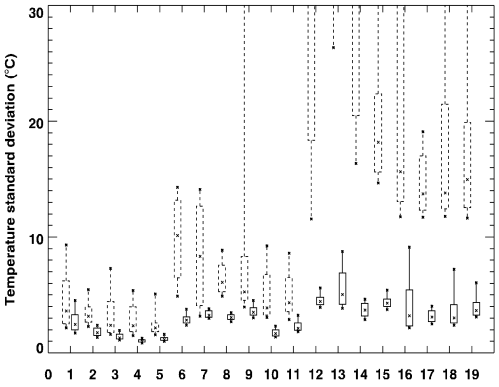

Figure 2 : Box-and-Whisker plot of the temperature standard deviation in the septum without (dashed) and with (solid) correction. Temperature levels values corresponding to 10% (lowest point), first quartile (lower box limit), median (cross), third quartile (higher box limit) and 90% (highest point) of the distribution of the temperature standard deviation are plotted for each volunteer.

Results

Figure 1 shows the temperature standard deviation (TSD) images obtained without (A) and with (B) the proposed correction. Most of the pixels show a standard deviation lower than 2°C after correction. However, the uncertainty of the temperature remained high in the region near the liver/heart/lung interface as shown in the lower right part of the image B. Figure 2 displays the distribution of the standard deviation values of the temperature for each volunteer in a ROI surrounding the septum. Without correction, the TSD median values varied from 2.18°C to 55.2°C, whereas after correction these values ranged between 1.01°C and 5.05°C. Moreover, 75% of the pixels within the septum were below 5°C in 17/19 cases. Computation time per image was 100 ms on a dual processor (INTEL 3.1 GHz Pentium, four cores) workstation equipped with 8 GB of RAM, demonstrating that our method is compatible with online temperature monitoring.

Discussion

Combination of slice tracking, cardiac triggering, efficient image registration and modeling of susceptibility changes related to motion allowed for significant improvements of the precision of the thermometry in the heart, with a temporal resolution given by the cardiac period (~1 second). The resulting standard deviation of the temperature was acceptable in view of local temperature increases achieved during cardiac catheter ablation. The proposed correction method was efficient to improve the precision of the thermometry in the septum and in the upper part of the liver. However, regions located near the lung/liver/heart interface still suffer from important temperature standard deviation values, probably due to the limited accuracy of the linear modeling of the magnetic field changes with motion in this region.

References

[1] Jais P et al, Arch Mal Coeur Vaiss 1995., [2] Quesson et al, Proc. ISMRM, Miami, 2005., [3] Isihara Y. et al, Proc. ISMRM, Berlin, 1992.